Published in final edited form as:
Arch Ophthalmol. 2011 November ; 129(11): 1466–1474. doi:10.1001/archophthalmol.2011.309.

Aceruloplasminemia: Retinal Histopathology and Iron-mediated Melanosome Degradation

Natalie Wolkow, B.S.[1], **Ying Song, M.D.**[1], **Ting-Di Wu, Ph.D.**[2,3], **Jiang Qian, M.D., Ph.D.**[4], **Jean-Luc Guerquin-Kern, Ph.D.**[2,3], and **Joshua L. Dunaief, M.D., Ph.D.**[1,*]

[1]F.M. Kirby Center for Molecular Ophthalmology, Scheie Eye Institute, Perelman School of Medicine at the University of Pennsylvania, Philadelphia, PA

[2]Institut Curie, Laboratoire de Microscopie Ionique, 91405-Orsay, France

[3]INSERM, U759, 91405-Orsay, France

[4]Dept. Pathology and Lab Med/APS, Albany Med College/Center, Albany, NY 12208

Abstract

Objective—To present, for the first time, the retinal histopathology of aceruloplasminemia, an autosomal recessive disease caused by mutation of the ferroxidase ceruloplasmin resulting in tissue iron overload.

Methods—Morphology of the human aceruloplasminemia retina was studied with light and electron microscopy. Retinal iron accumulation was assessed with Perls' Prussian blue staining, immunohistochemistry and secondary ion mass spectrometry.

Results—Light and electron microscopic analysis revealed several ocular pathologic findings that resembled age-related macular degeneration, including retinal pigment epithelium depigmentation, atrophy and hypertrophy, nodular and diffuse drusen, lipofuscin and melanolipofuscin granules. Complement deposition was detected in drusen. The retinal pigment epithelial cells and neural retina had increased levels of iron. Two major types of retinal pigment epithelial cells were observed: melanosome-rich and melanosome-poor. Melanosome-rich cells had increased levels of iron and melanolipofuscin. The melanolipofuscin granules were observed in large aggregates where some of the melanosomes were degrading. Melanosome-poor cells lacked melanosomes, melanolipofuscin and lipofuscin, but contained electron dense aggregates high in iron, phosphorus and sulfur.

Conclusion—The findings in the aceruloplasminemia retina resemble some of those found in age-related macular degeneration. Also, they suggest that retinal pigment epithelium melanosomes can be degraded via iron-mediated reactive oxygen species production.

[*]Corresponding author and requests for reprints. 305 Stellar Chance Labs, 422 Curie Blvd., Philadelphia, PA 19104; telephone number: 215-898-5235 fax: 215-573-3918 jdunaief@mail.med.upenn.edu.

Authors' contributions:
N.W. and J.D developed the experimental plans and wrote the manuscript. J.Q. performed the enucleation and fixation. N.W. and Y.S. did the PAS, Perls' and immunohistochemistry experiments and analysis. NW did the EM analysis. J-L. G-K. and T-D. W. performed the SIMS analysis. N. W. prepared all figures. All authors revised and edited the manuscript.

Clinical Relevance—Mechanisms underlying the pathology found in aceruloplasminemia may also be important in age-related macular degeneration.

Keywords

Aceruloplasminemia; ceruloplasmin; ferroxidase; iron; retina; retinal pigment epithelium; age-related macular degeneration; melanosome; melanin; NanoSIMS

INTRODUCTION

Aceruloplasminemia (aCP) is a very rare autosomal recessive disease (1) caused by mutation of the ceruloplasmin gene (2). Aceruloplasminemia is characterized by a triad of diabetes, retinal degeneration and neurodegeneration that usually manifests between the ages 30–55 (3–5). The disease is caused by iron accumulation in the pancreas, liver, brain and retina, due to a decrease in iron export (4–6).

Ceruloplasmin (Cp) is a ferroxidase protein that is either secreted from cells or GPI-linked to the outer surface of cell membranes (7). Cp interacts with ferroportin (Fpn), the cellular iron exporter, to export ferrous (Fe^{2+}) iron from cells (8). As a ferroxidase, Cp converts ferrous (Fe^{2+}) to ferric (Fe^{3+}) iron, allowing ferric iron to bind to transferrin in the plasma (8). Lack of Cp, even in the presence of Fpn, markedly impairs iron export from cells (9). Thus, ferroxidases are necessary components for iron export.

In AMD retinas, iron and transferrin levels are elevated, suggesting that iron toxicity may contribute to age-related macular degeneration (AMD) pathogenesis (10, 11). Further, in mice, combined knockout of Cp and its homologue, Hephaestin, causes retinal and brain iron accumulation and degeneration (12, 13). The retinal degeneration resembles AMD (13).

Pathologic studies of many aCP tissues have been published (3–5); however, no study has examined the retinal histopathology. The only published reports focusing on the retina have been clinical case reports. These have shown pigmentary abnormalities in the peripheral retina (14, 15). In 2005, we published a clinical report of an individual with aCP (15). In the current study we examine the retinal histopathology of the same individual at age 60.

METHODS

TISSUE PREPARATION

Eyes were obtained from a 60 year old aCP male donor after a 7 hour *postmortem* interval in accordance with the Declaration of Helsinki. At the time of the previous study (15), the donor had iron deficiency anemia, longstanding diabetes, cardiomyopathy, liver iron accumulation, dementia and a macular degeneration characterized by drusen and areas of RPE depigmentation (15). Subsequent to the published report, he had many hypoglycemic episodes, developed renal failure, was hospitalized, developed aspiration pneumonia, became septic and died. For the current studies, samples from the anterior segment, retina/choroid/sclera and optic nerve of his right eye were used. As normal control, an eye from a 60 year old male donor, with a 7 hour *postmortem* interval, and no history of retinal disease was obtained from the Lions Eye Bank. An AMD control eye was obtained from the CAPT

Eye Donor Program in collaboration with FFB from an 86-year old female with a history of AMD; the post-mortem interval for this eye was 20 hours. All eyes were fixed in formalin, embedded in paraffin and sectioned at 7-μm thickness.

PERIODIC ACID SCHIFF'S STAINING

Paraffin sections from the ocular regions indicated above were stained using the Periodic Acid Schiff's Stain Kit from Polysciences (Warrington, PA) as suggested by the manufacturer. Images were acquired on a Nikon Eclipse TE300 (Japan) using Image-Pro Plus 6.1. Histopathology was analyzed as described (16).

PERLS' STAINING FOR IRON

Paraffin sections were bleached with 0.25% $KMnO_4$ and 0.5% oxalic acid, then stained with 5% $K_4Fe(CN)_6$ and 5%HCl for 30 minutes.

IMMUNOHISTOCHEMISTRY

Paraffin sections were stained using the Vectastain ABC Alkaline Phosphatase for Rabbit and Mouse IgG and Vector BCIP-NBT kits (Vector Laboratories, Burlingame, CA). Primary antibodies for L-ferritin (F-17, gift of P. Arosio and P. Santambrogio, Italy), C5b-9 (#M0777, DAKO) and vitronectin (#MAB1945, Millipore) were used at 1:100 dilutions.

ELECTRON MICROSCOPY

The temporal macula was post-fixed with osmium tetroxide, dehydrated, and embedded in EPON. Thin sections were stained and examined with a JEOL1010 TEM. Images were acquired with AMT Image Capture software and were rotated and cropped with Adobe Photoshop.

QUANTIFICATION OF MELANOSOMES, LYSOSOMES AND COMPLEX GRANULES

Images of 16 consecutive melanosome-poor and 16 melanosome-rich RPE cells were taken at ×10,000 magnification on a previously un-examined section. RPE granules were quantified as previously described (17).

SECONDARY ION MASS SPECTROMETRY

Secondary ion mass spectrometry (SIMS) is used to analyze the spatial distribution of elements in a sample at a resolution of up to 50nm (18). Samples for SIMS analysis were prepared as for TEM, but with some modifications. Samples were not post-fixed in osmium tetroxide, and sections were not stained with uranyl acetate or lead citrate. Thin (40nm) and thick (150nm) sections were cut, and were imaged with a JEOL1010 TEM, then analyzed with a NanoSIMS-50 ion microprobe (CAMECA, Gennevilliers, France) operating in scanning mode.

RESULTS

To determine if the aCP eye had any unique pathologic changes, it was examined at the gross, light microscopic (LM) and the electron microscopic (EM) levels. At the gross level,

the phakic right eye had no abnormalities other than macular degeneration consistent with the previous clinical report (15).

At the LM level, the cornea, iris, ciliary body and optic nerve had normal morphology (data not shown). Both peripheral and macular neural retina were normal (Fig 1A and B), but the RPE and Bruch's membrane contained many pathologic changes on all sections examined, similar to pathology previously described in AMD (16). Nodular drusen (16, 19–21) were present in both the periphery and macula (Fig 1C), although they were much more frequent in the periphery. The periphery also had many diffuse drusen (16, 19, 20) (Fig 1D), while the macula had none. The macula had sub-retinal drusenoid deposits (22, 23) (Fig 1E); the periphery did not. Both macula and periphery had RPE cells with inclusions (16) (21) (Fig 1F), and RPE cells that had extruded from the normal RPE layer (16, 24) (Fig 1G). The macula had several areas of RPE hypertrophy (16) (Fig 1H) and atrophy (16) (Fig 1I); the periphery did not. Both macula and periphery had areas of depigmented RPE cells that lacked the brown color of their neighbors, and instead stained purple (Fig 1J and K); control normal and AMD RPE cells lacked this color variation (Fig 1L and M).

At the EM level, drusen and basal linear deposits resembled deposits previously described in AMD (16, 25–27) (Figure 2A–E). Also, similar to AMD, aCP drusen had evidence of complement activation (28–31) (Figure 3A–C).

To determine if iron had accumulated in any cells, Perls' stain was performed. Strong label was seen in the RPE of both the periphery and macula (Fig 4C–J) but the periphery did not have as many Perls' positive cells. Hypertrophic RPE cells were always Perls' positive (Fig 4J). The neural retina, choroid, optic nerve, ciliary body, iris, trabecular meshwork and cornea were Perls' negative (data not shown). Interestingly, many RPE cells that subsequently had strong Perls' label could never be fully bleached, but retained a golden color, presumably from the high iron accumulation (Fig 4G–J).

To determine if the neural retina and Perls' negative RPE cells had increased iron levels compared to controls, immunohistochemistry for L-ferritin, the iron storage protein, was performed. The neural retina (Fig 5F) and both peripheral and macular RPE cells had strong L-ferritin stain, more than normal control (Fig 5G–N). In normal and aCP RPE, the macula had more L-ferritin stain than the periphery (Fig 5G–N). Although the aCP macula had strong L-ferritin label, the golden cells with large iron deposits did not stain strongly with L-ferritin, suggesting that iron in them may not stored as ferritin (Fig 5L and N).

To determine if increased iron levels affected the normal RPE cytoarchitecture, cells were examined with EM. The aCP RPE mitochondria had abnormal electron dense inclusions (Fig 6C and F). Normal RPE lacked these inclusions (Fig 6A and D), while AMD RPE had occasional inclusions (Fig 6B and E). Such inclusions have not been previously described in RPE mitochondria (27, 24). SIMS analysis detected no increase in iron in the inclusions above the background tissue level, suggesting that the inclusions are areas of damaged lipids or proteins and not areas of significant iron deposits (data not shown).

EM of unstained sections revealed two major kinds of RPE cells, melanosome-poor cells that had many electron dense particles (Fig 7A, arrows), and melanosome-rich cells that

lacked the electron dense particles (Fig 7A, arrowheads). Such particles were never seen in AMD and normal controls (data not shown) and have not been previously reported (17, 27, 32). Stained sections revealed melanosome-rich, melanosome-poor, and a few intermediate cells, suggesting a possible progression from the melanosome-rich to poor phenotype over time (Fig 7 B–D).

In addition to melanosomes, the melanosome-rich cells contained lipofuscin and complex granules, all structures seen in AMD and with ageing (Fig 7E) (17, 32). For 16 melanosome-rich RPE cells, the average number ± SD of melanosomes, lipofuscin and complex granules per cellular cross-section was 20±7.8, 35±12 and 11±6.1, respectively.

In the melanosome-rich cells, a progression from normal melanosomes to large aggregates of melanosomes in lipofuscinoid material was observed (Fig 7F–L). The melanosomes in these aggregates could be intact (Fig 7J) or in different states of degradation (Fig 7K, L). Intermediate cells contained aggregates of degrading melanosomes, but many more of them. In most cases, intact melanosomes could no longer be distinguished (Fig 7M). Aggregates with degrading melanosomes were not observed in normal or AMD controls (data not shown).

Melanosome-poor RPE, lacked melanosomes, lipofuscin and complex granules. For 16 melanosome-poor RPE cells the average number ± SD of melanosomes, lipofuscin and complex granules per cell profile was 1.8±2.8, 1.0±1.5 and 0.8±1.4, respectively. Melanosomes and complex granules were never seen outside the RPE in the pre-RPE or sub-RPE spaces, suggesting that melanosomes had not been extruded, but had been degraded. Melanosome-poor RPE had many electron-dense, irregularly shaped membrane-bound granules that resembled siderosomes (33, 34) (Fig 7N–P). Such granules were never seen in normal or AMD RPE (data not shown), and have not been previously described in RPE (17, 27, 32).

To determine the subcellular location of iron in the RPE, unstained sections were examined with EM and SIMS. Complex granules from melanosome-rich aCP RPE had thin, grainy electron dense borders (Fig 8A, arrowheads), while similar granules from normal and AMD RPE lacked these borders (data not shown). Melanosome-rich aCP RPE also had vesicles with granular electron-dense material (Fig 8A, arrow), while normal and AMD cells did not (data not shown). SIMS analysis demonstrated that the grainy borders on the outer edges of the complex and lipofuscin granules were iron, and as was the material in the vesicles (Fig 8A arrow, 8D, E). Melanosomes contained some iron and high sulfur levels (Fig 8C–F).

The melanosome-poor cells had only siderosomes (Fig 8G) that contained very high amounts of iron, phosphorus and sulfur (Fig 8G, J, K). Compared to melanosome-rich cells, this iron content was much higher (Fig 8M, N).

DISCUSSION

We have presented for the first time the retinal histopathology of aceruloplasminemia, and evidence for iron-mediated melanosome degradation. The aCP eye had many similarities to AMD, but also notable differences. Since this subject died at age 60, it is possible that some

of the AMD-like changes were the result of aging or AMD; however, pathology was clinically evident from age 47, suggesting that most of our findings are the result of aCP (15).

As in AMD, RPE depigmentation, atrophy, hypertrophy, inclusions and extrusion were observed (Figure 1) (16). The morphology of these was similar to what is seen in AMD; however, the extent of depigmentation was greater than in AMD. Depigmented cells are found mostly in the AMD macula, while in aCP they were present in both the macula and periphery (16).

The aCP eye had drusen, basal linear deposits and deposits in the subretinal space (Figure 1 and 2) (22, 27). Although the deposit morphology was similar to AMD at both LM and EM levels (16, 25, 26), the distribution differed from what is typical of AMD. The aCP eye had many drusen in the periphery and fewer in the macula, while the opposite is true in AMD (20, 16, 35). The aCP eye also had a greater number of sub-retinal drusenoid deposits in the macula than is typical of AMD (22).

In AMD, drusen contain activated complement. C5b-9 (MAC), the terminal component of the complement cascade, is present in most AMD nodular and diffuse drusen in a mottled pattern (29, 36). ACP drusen were positive for C5b-9 and had the expected mottled pattern; however, not all drusen labeled (data not shown). ACP diffuse drusen had more frequent C5b-9 staining than did nodular drusen, while in AMD staining is similar in both types (36).

Vitronectin, a plasma protein that inhibits the formation of the MAC, is present in high levels in all AMD drusen (28, 30), and is also seen in occasional RPE cells (30). Similar to AMD, vitronectin strongly labeled all aCP drusen and occasional RPE cells (Figure 3). Sub-retinal drusenoid deposits were negative for both C5b-9 and vitronectin (Figure 3).

AMD eyes have increased RPE iron levels compared to normal controls, as detected with enhanced Perls' stain (10). As in AMD, aCP RPE had increased iron levels; however, the levels were so high that they could be detected with un-enhanced Perls' stain in all sections (Figure 4). Some aCP RPE, especially in the macula, had so much iron that it was visible as a golden color that could not be bleached (Figure 4). The aCP macula had more iron than the periphery (Figure 4); the same was true of the normal retina (Figure 5), suggesting that RPE cells of the macula and periphery handle iron in different ways (37), or that RPE in different regions may be exposed to different iron levels. Whether there are similar regional differences in AMD has not been shown (10).

Because the aCP neural retina and some RPE cells did not stain with Perls', we used L-ferritin immunostaining as a more sensitive test for elevated iron levels. Since Cp is normally expressed by several retinal cells types, including Muller cells and retinal astrocytes, increased iron levels in the aCP neural retina were expected (38–40). Indeed, L-ferritin levels in the aCP retina were elevated (Figure 5). Additionally, aCP RPE from both the periphery and macula had greater L-ferritin levels than normal RPE (Figure 5). Interestingly, the golden, iron-laded RPE cells did not stain strongly for L-ferritin. Rather, neighboring cells that lacked the golden deposits had high levels of L-ferritin (Figure 5),

suggesting that iron in the aCP RPE cells may be present in two forms, ferritin and hemosiderin.

As cells accumulate iron they first store it in ferritin. Once the ferritin system becomes overwhelmed, iron is stored as hemosiderin in siderosomes (33, 41). Hemosiderin is a large, irregularly-shaped, insoluble, crystalline aggregate of iron and other minerals; the iron comes from the cores of degraded ferritin molecules (33, 42). Immuno-EM studies have demonstrated that ferritin label in siderosomes is weak because it is degraded since ferritin is degraded (43). In the aCP eye, the irregularly-shaped granules resembled siderosomes (Fig 7 and 8) (34, 44, 45). This explains why the iron-laden golden RPE had lower than expected levels of ferritin. The difference in RPE macular and peripheral subcellular iron distribution may help explain the discrepancy in drusen distribution in aCP and AMD eyes. Iron distribution in AMD maculas is more similar to the aCP periphery than the aCP macula. Thus, the aCP periphery may better represent iron loading in AMD.

ACP RPE cells had mitochondrial pathology (Figure 6). The majority of aCP mitochondria had at least one large focus of electron dense material that was not iron, but likely damaged lipid and protein. The AMD eye, which had a longer post-mortem interval than the aCP eye, had only occasional mitochondrial accumulations, and they were much smaller than those in aCP. The presence mitochondrial damage in aCP supports previous biochemical studies on aCP brains, which demonstrated mitochondrial dysfunction of respiratory chain complexes I and IV (46–48).

Melanosomes, lipofuscin and complex granules of aCP RPE also differed from AMD and normal (Figure 7, 8) (32). A typical macular RPE cell from a normal 60 year old eye has 17–20 lipofuscin, 11–13 melanin, and 9–14 complex granules per cell profile (17). The aCP RPE macula contained two types of cells, melanosome-rich and melanosome-poor, both with abnormal numbers of granules. Melanosome-rich RPE had greater than expected numbers of lipofuscin granules and melanosomes per cell profile, 35 and 20, respectively, but normal numbers of complex granules. The melanosome-poor cells, on the other hand, had significantly lower numbers of each granule type, approximately one of each per cell profile, suggesting that the melanosomes may have been degraded.

Melanosome degradation in RPE is controversial (49), mainly because there has been limited *in vivo* evidence (49–51). Melanosome degradation has been described in fetal bovine RPE cells as the tapetum lucidum becomes amelanotic (50, 51). The melanosomes in the tapetal RPE form aggregates of degrading melanosomes (50), similar to the aggregates of degrading melanosomes that we observed in the aCP RPE (Figure 7). The mechanism of melanosome degradation in the tapetal RPE is not clear. The authors of the study and other contemporaneous studies (32, 52, 53) suggest that the presence of lysosomal enzymes in melanosomes implies melanosome degradation by lysosomes. However, it is now known that melanosomes are lysosome-related organelles that normally contain lysosomal enzymes and cannot be easily degraded (49, 54, 55).

Melanosomes can, however, be photodegraded (56, 57) and degraded with hydrogen peroxide (49, 58). Moreover, *in vitro* experiments have shown that the rate of synthetic

melanin degradation is dramatically increased when iron or copper is added to the reaction (58). Abundant iron in the melanosomes, lipofuscin and complex granules of aCP RPE (Fig 7, 8) suggests that melanosomes may disappear from RPE because of iron-mediated degradation. Melanosomes in melanosome-rich RPE contain very high levels of sulfur (Figure 8), while melanosome-poor RPE cells have high sulfur levels in the siderosomes, suggesting that components of degraded melanosomes are present in the hemosiderin. Thus, the aCP RPE cells may be an *in vivo* example of what has been observed *in vitro*.

In conclusion, our studies have shown that RPE cells are greatly affected by the loss of Cp; they accumulate iron, and develop an AMD-like pathology with many unique features.

Acknowledgments

For funding, we thank the NIH (RO1EY015240, 1F30AG037289-01,EY012211, EY012261, and EY012279), an unrestricted grant from Research to Prevent Blindness, the F.M. Kirby Foundation, a gift from L. Stanley Mauger in memory of Lee F. Mauger, MD, and the Paul and Evanina Bell Mackall Foundation Trust. We also thank the PICT-IBiSA imaging facility in the Institut Curie. And, we thank Ray Meade at the University of Pennsylvania Electron Microscopy Resource Laboratory for outstanding technical assistance. Joshua L. Dunaief had full access to all the data in the study and takes responsibility for the integrity of the data and the accuracy of the data analysis.

References

1. Miyajima H, Kohno S, Takahashi Y, Yonekawa O, Kanno T. Estimation of the gene frequency of aceruloplasminemia in japan. Neurology. 1999 Aug 11; 53(3):617–619. [PubMed: 10449129]
2. Yoshida K, Furihata K, Takeda S, et al. A mutation in the ceruloplasmin gene is associated with systemic hemosiderosis in humans. Nat Genet. 1995 Mar; 9(3):267–272. [PubMed: 7539672]
3. Miyajima H, Nishimura Y, Mizoguchi K, Sakamoto M, Shimizu T, Honda N. Familial apoceruloplasmin deficiency associated with blepharospasm and retinal degeneration. Neurology. 1987 May; 37(5):761–767. [PubMed: 3574673]
4. Morita H, Ikeda S, Yamamoto K, et al. Hereditary ceruloplasmin deficiency with hemosiderosis: A clinicopathological study of a japanese family. Ann Neurol. 1995 May; 37(5):646–656. [PubMed: 7755360]
5. Miyajima H. Aceruloplasminemia, an iron metabolic disorder. Neuropathology. 2003 Dec; 23(4): 345–350. [PubMed: 14719552]
6. Harris ZL, Durley AP, Man TK, Gitlin JD. Targeted gene disruption reveals an essential role for ceruloplasmin in cellular iron efflux. Proc Natl Acad Sci U S A. 1999 Sep 14; 96(19):10812–10817. [PubMed: 10485908]
7. Patel BN, David S. A novel glycosylphosphatidylinositol-anchored form of ceruloplasmin is expressed by mammalian astrocytes. J Biol Chem. 1997 Aug 8; 272(32):20185–20190. [PubMed: 9242695]
8. De Domenico I, Ward DM, di Patti MC, et al. Ferroxidase activity is required for the stability of cell surface ferroportin in cells expressing GPI-ceruloplasmin. EMBO J. 2007 Jun 20; 26(12):2823–2831. [PubMed: 17541408]
9. McKie AT, Marciani P, Rolfs A, et al. A novel duodenal iron-regulated transporter, IREG1, implicated in the basolateral transfer of iron to the circulation. Mol Cell. 2000 Feb; 5(2):299–309. [PubMed: 10882071]
10. Hahn P, Milam AH, Dunaief JL. Maculas affected by age-related macular degeneration contain increased chelatable iron in the retinal pigment epithelium and bruch's membrane. Arch Ophthalmol. 2003 Aug; 121(8):1099–1105. [PubMed: 12912686]
11. Chowers I, Wong R, Dentchev T, et al. The iron carrier transferrin is upregulated in retinas from patients with age-related macular degeneration. Invest Ophthalmol Vis Sci. 2006 May; 47(5): 2135–2140. [PubMed: 16639025]

12. Hahn P, Qian Y, Dentchev T, et al. Disruption of ceruloplasmin and hephaestin in mice causes retinal iron overload and retinal degeneration with features of age-related macular degeneration. Proc Natl Acad Sci U S A. 2004 Sep 21; 101(38):13850–13855. [PubMed: 15365174]

13. Hadziahmetovic M, Dentchev T, Song Y, et al. Ceruloplasmin/hephaestin knockout mice model morphologic and molecular features of AMD. Invest Ophthalmol Vis Sci. 2008 Jun; 49(6):2728–2736. [PubMed: 18326691]

14. Yamaguchi K, Takahashi S, Kawanami T, Kato T, Sasaki H. Retinal degeneration in hereditary ceruloplasmin deficiency. Ophthalmologica. 1998; 212(1):11–14. [PubMed: 9438577]

15. Dunaief JL, Richa C, Franks EP, et al. Macular degeneration in a patient with aceruloplasminemia, a disease associated with retinal iron overload. Ophthalmology. 2005 Jun; 112(6):1062–1065. [PubMed: 15882908]

16. Bressler NM, Silva JC, Bressler SB, Fine SL, Green WR. Clinicopathologic correlation of drusen and retinal pigment epithelial abnormalities in age-related macular degeneration. Retina. 1994; 14(2):130–142. [PubMed: 8036323]

17. Feeney-Burns L, Hilderbrand ES, Eldridge S. Aging human RPE: Morphometric analysis of macular, equatorial, and peripheral cells. Invest Ophthalmol Vis Sci. 1984 Feb; 25(2):195–200. [PubMed: 6698741]

18. Guerquin-Kern JL, Wu TD, Quintana C, Croisy A. Progress in analytical imaging of the cell by dynamic secondary ion mass spectrometry (SIMS microscopy). Biochim Biophys Acta. 2005 Aug 5; 1724(3):228–238. [PubMed: 15982822]

19. Green WR, McDonnell PJ, Yeo JH. Pathologic features of senile macular degeneration. Ophthalmology. 1985 May; 92(5):615–627. [PubMed: 2409504]

20. Spraul CW, Grossniklaus HE. Characteristics of drusen and bruch's membrane in postmortem eyes with age-related macular degeneration. Arch Ophthalmol. 1997 Feb; 115(2):267–273. [PubMed: 9046265]

21. Sarks SH, Arnold JJ, Killingsworth MC, Sarks JP. Early drusen formation in the normal and aging eye and their relation to age related maculopathy: A clinicopathological study. Br J Ophthalmol. 1999 Mar; 83(3):358–368. [PubMed: 10365048]

22. Rudolf M, Malek G, Messinger JD, Clark ME, Wang L, Curcio CA. Sub-retinal drusenoid deposits in human retina: Organization and composition. Exp Eye Res. 2008 Nov; 87(5):402–408. [PubMed: 18721807]

23. Sarks JP, Sarks SH, Killingsworth MC. Evolution of soft drusen in age-related macular degeneration. Eye (Lond). 1994; 8(Pt 3):269–283. (Pt 3). [PubMed: 7525362]

24. Sarks SH. Ageing and degeneration in the macular region: A clinico-pathological study. Br J Ophthalmol. 1976 May; 60(5):324–341. [PubMed: 952802]

25. Burns RP, Feeney-Burns L. Clinico-morphologic correlations of drusen of bruch's membrane. Trans Am Ophthalmol Soc. 1980; 78:206–225. [PubMed: 6167054]

26. Feeney-Burns L, Ellersieck MR. Age-related changes in the ultrastructure of bruch's membrane. Am J Ophthalmol. 1985 Nov 15; 100(5):686–697. [PubMed: 4061550]

27. Hogan, MJ.; Alvarado, JA.; Weddell, JE. Histology of the human eye; an atlas and textbook. Philadelphia: Saunders; 1971.

28. Hageman GS, Mullins RF, Russell SR, Johnson LV, Anderson DH. Vitronectin is a constituent of ocular drusen and the vitronectin gene is expressed in human retinal pigmented epithelial cells. FASEB J. 1999 Mar; 13(3):477–484. [PubMed: 10064614]

29. Johnson LV, Ozaki S, Staples MK, Erickson PA, Anderson DH. A potential role for immune complex pathogenesis in drusen formation. Exp Eye Res. 2000 Apr; 70(4):441–449. [PubMed: 10865992]

30. Johnson LV, Leitner WP, Staples MK, Anderson DH. Complement activation and inflammatory processes in drusen formation and age related macular degeneration. Exp Eye Res. 2001 Dec; 73(6):887–896. [PubMed: 11846519]

31. Anderson DH, Radeke MJ, Gallo NB, et al. The pivotal role of the complement system in aging and age-related macular degeneration: Hypothesis re-visited. Prog Retin Eye Res. 2010 Mar; 29(2):95–112. [PubMed: 19961953]

32. Feeney L. Lipofuscin and melanin of human retinal pigment epithelium. fluorescence, enzyme cytochemical, and ultrastructural studies. Invest Ophthalmol Vis Sci. 1978 Jul; 17(7):583–600. [PubMed: 669890]
33. Wixom RL, Prutkin L, Munro HN. Hemosiderin: Nature, formation, and significance. Int Rev Exp Pathol. 1980; 22:193–225. [PubMed: 7005144]
34. Richter GW. Studies of iron overload. rat liver siderosome ferritin. Lab Invest. 1984 Jan; 50(1):26–35. [PubMed: 6694350]
35. Abdelsalam A, Del Priore L, Zarbin MA. Drusen in age-related macular degeneration: Pathogenesis, natural course, and laser photocoagulation-induced regression. Surv Ophthalmol. 1999 Jul-Aug;44(1):1–29. [PubMed: 10466585]
36. Mullins RF, Russell SR, Anderson DH, Hageman GS. Drusen associated with aging and age-related macular degeneration contain proteins common to extracellular deposits associated with atherosclerosis, elastosis, amyloidosis, and dense deposit disease. FASEB J. 2000 May; 14(7): 835–846. [PubMed: 10783137]
37. Burke JM, Hjelmeland LM. Mosaicism of the retinal pigment epithelium: Seeing the small picture. Mol Interv. 2005 Aug; 5(4):241–249. [PubMed: 16123538]
38. Klomp LW, Farhangrazi ZS, Dugan LL, Gitlin JD. Ceruloplasmin gene expression in the murine central nervous system. J Clin Invest. 1996 Jul 1; 98(1):207–215. [PubMed: 8690795]
39. Klomp LW, Gitlin JD. Expression of the ceruloplasmin gene in the human retina and brain: Implications for a pathogenic model in aceruloplasminemia. Hum Mol Genet. 1996 Dec; 5(12): 1989–1996. [PubMed: 8968753]
40. Levin LA, Geszvain KM. Expression of ceruloplasmin in the retina: Induction after optic nerve crush. Invest Ophthalmol Vis Sci. 1998 Jan; 39(1):157–163. [PubMed: 9430557]
41. Harrison PM, Arosio P. The ferritins: Molecular properties, iron storage function and cellular regulation. Biochim Biophys Acta. 1996 Jul 31; 1275(3):161–203. [PubMed: 8695634]
42. Koorts AM, Viljoen M. Ferritin and ferritin isoforms I: Structure-function relationships, synthesis, degradation and secretion. Arch Physiol Biochem. 2007 Feb; 113(1):30–54. [PubMed: 17522983]
43. Cooper PJ, Iancu TC, Ward RJ, Guttridge KM, Peters TJ. Quantitative analysis of immunogold labelling for ferritin in liver from control and iron-overloaded rats. Histochem J. 1988 Sep; 20(9): 499–509. [PubMed: 3240951]
44. Richter GW. Electron microscopy of hemosiderin presence of ferritin and occurrence of crystalline lattices in hemosiderin deposits. J Biophys Biochem Cytol. 1958 Jan 25; 4(1):55–58. [PubMed: 13502428]
45. Iancu TC. Ferritin and hemosiderin in pathological tissues. Electron Microsc Rev. 1992; 5(2):209–229. [PubMed: 1581551]
46. Yoshida K, Kaneko K, Miyajima H, et al. Increased lipid peroxidation in the brains of aceruloplasminemia patients. J Neurol Sci. 2000 Apr 15; 175(2):91–95. [PubMed: 10831768]
47. Miyajima H, Kono S, Takahashi Y, Sugimoto M. Increased lipid peroxidation and mitochondrial dysfunction in aceruloplasminemia brains. Blood Cells Mol Dis. 2002 Nov-Dec;29(3):433–438. [PubMed: 12547232]
48. Kohno S, Miyajima H, Takahashi Y, Suzuki H, Hishida A. Defective electron transfer in complexes I and IV in patients with aceruloplasminemia. J Neurol Sci. 2000 Dec 15; 182(1):57–60. [PubMed: 11102640]
49. Borovansky J, Elleder M. Melanosome degradation: Fact or fiction. Pigment Cell Res. 2003 Jun; 16(3):280–286. [PubMed: 12753402]
50. Feeney-Burns L, Mixon RN. Development of amelanotic retinal pigment epithelium in eyes with a tapetum lacidum: Melanosome autophagy and termination of melanogenesis. Dev Biol. 1979 Sep; 72(1):73–88. [PubMed: 510782]
51. Garcia RI, Flynn EA, Szabo G. Autophagocytosis of melanosomes in cultured embryonic retinal pigment cells. Experientia. 1983 Apr 15; 39(4):391–392. [PubMed: 6832319]
52. Feeney-Burns L, Gao CL, Tidwell M. Lysosomal enzyme cytochemistry of human RPE, bruch's membrane and drusen. Invest Ophthalmol Vis Sci. 1987 Jul; 28(7):1138–1147. [PubMed: 3596992]

53. Kim IT, Choi JB. Melanosomes of retinal pigment epithelium--distribution, shape, and acid phosphatase activity. Korean J Ophthalmol. 1998 Dec; 12(2):85–91. [PubMed: 10188367]

54. Raposo G, Marks MS. Melanosomes--dark organelles enlighten endosomal membrane transport. Nat Rev Mol Cell Biol. 2007 Oct; 8(10):786–797. [PubMed: 17878918]

55. Bhatnagar V, Anjaiah S, Puri N, Darshanam BN, Ramaiah A. pH of melanosomes of B 16 murine melanoma is acidic: Its physiological importance in the regulation of melanin biosynthesis. Arch Biochem Biophys. 1993 Nov 15; 307(1):183–192. [PubMed: 8239655]

56. Zareba M, Szewczyk G, Sarna T, et al. Effects of photodegradation on the physical and antioxidant properties of melanosomes isolated from retinal pigment epithelium. Photochem Photobiol. 2006 Jul-Aug;82(4):1024–1029. [PubMed: 17205626]

57. Sarna T, Burke JM, Korytowski W, et al. Loss of melanin from human RPE with aging: Possible role of melanin photooxidation. Exp Eye Res. 2003 Jan; 76(1):89–98. [PubMed: 12589778]

58. Korytowski W, Sarna T. Bleaching of melanin pigments. role of copper ions and hydrogen peroxide in autooxidation and photooxidation of synthetic dopa-melanin. J Biol Chem. 1990 Jul 25; 265(21):12410–12416. [PubMed: 2165063]

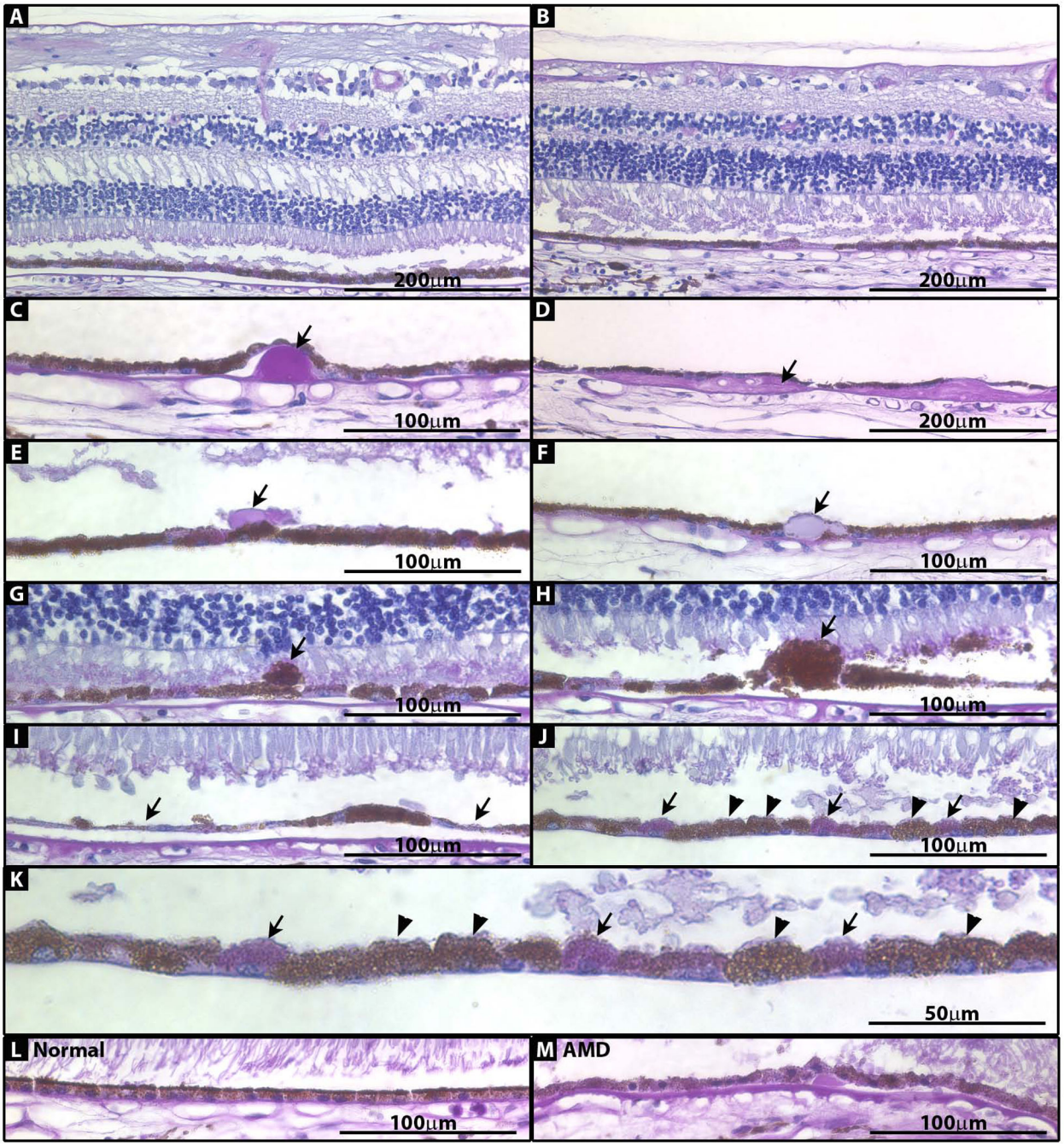

Figure 1. Photomicrographs of paraffin-embedded sections of peripheral and macular retina stained with PAS/hematoxylin

(A) Macula. (B) Periphery. (C) Nodular druse (arrow) from periphery. (D) Diffuse druse (arrow) from periphery. (E) Subretinal drusenoid deposit (arrow) from macula. (F) RPE inclusion (arrow) from periphery. (G) Extruded RPE cell (arrow) from macula. (H) Hypertrophic RPE cell (arrow) from macula. (I) RPE thinning/atrophy (arrows) in macula. (J) Areas of pigmented (arrowhead) and depigmented (arrow) RPE cells. (K) Image in J enlarged. (L) RPE from normal control eye. (M) RPE from AMD control eye.

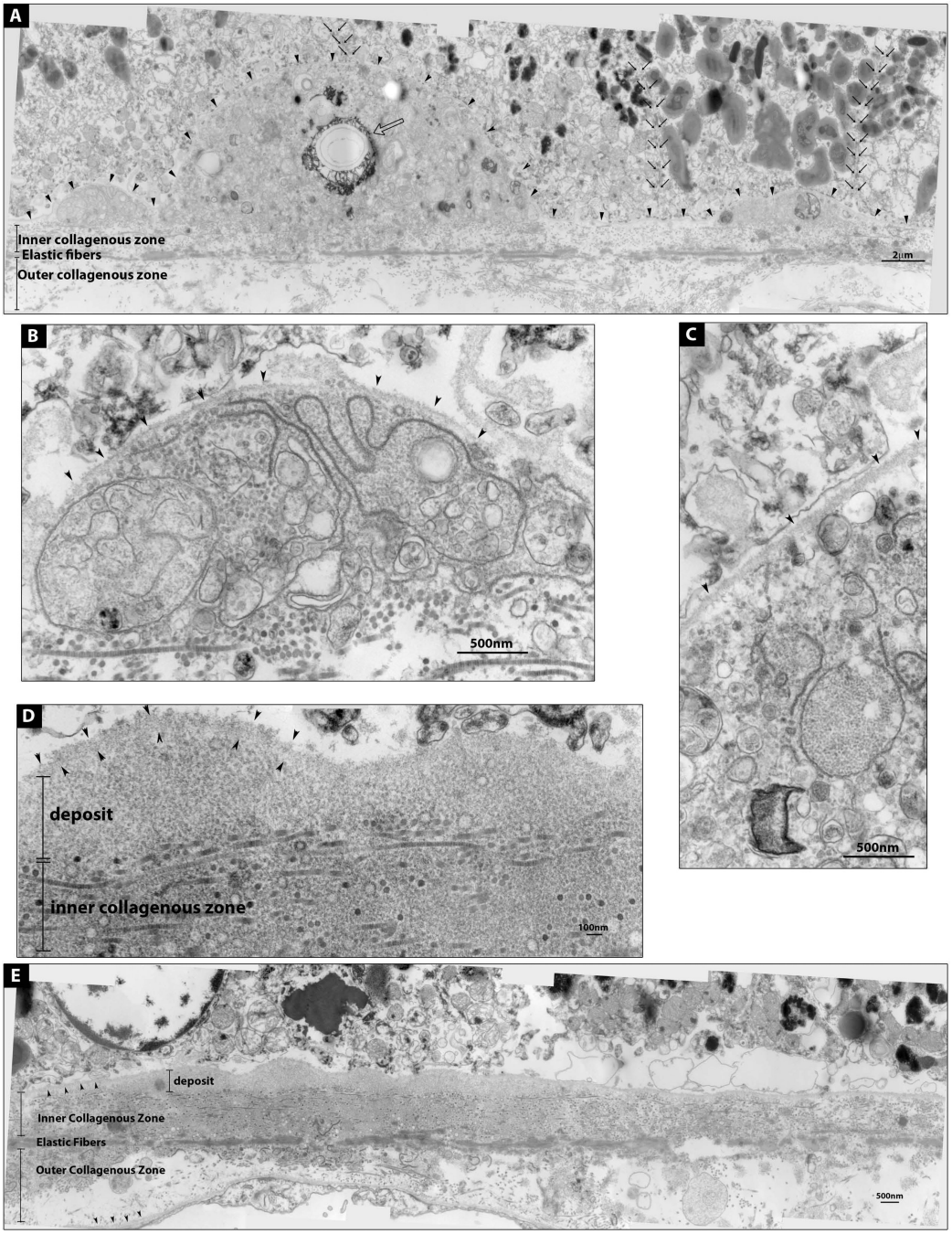

Figure 2. Electron micrographs of a druse and a basal linear deposit

(A) A Druse flanked by two deposits. RPE basal lamina is demarcated by arrowheads. These deposits contain membranous components and a crystallized area (open arrow). Both melanosome-rich and poor RPE cells sit on top of the deposits; cell boundaries are marked by small black arrows. (B and C) Enlarged images of the deposits in A. (D) Enlarged image of E; basal linear deposit containing homogenously granular material; RPE basal lamina (arrowheads). (E) Basal linear deposit. RPE and choroidal basal laminas are marked by arrowheads.

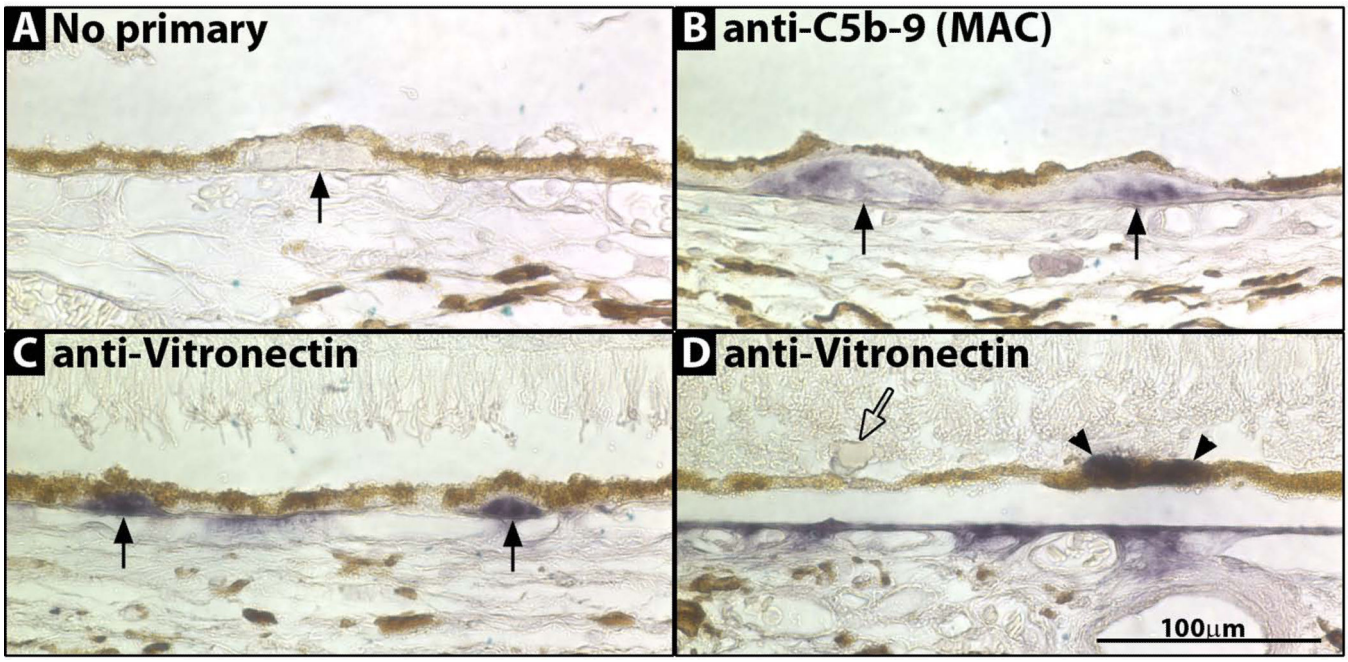

Figure 3. Photomicrographs of drusen immunostained for C5b-9 and vitronectin

(A) No primary antibody. Druse (arrow). (B) anti-C5b-9 (MAC) staining two drusen (arrows). (C) anti-vitronectin staining two drusen (arrows). (D) anti-vitronectin staining RPE (arrowheads) but not staining a sub-retinal drusenoid deposit (open arrow).

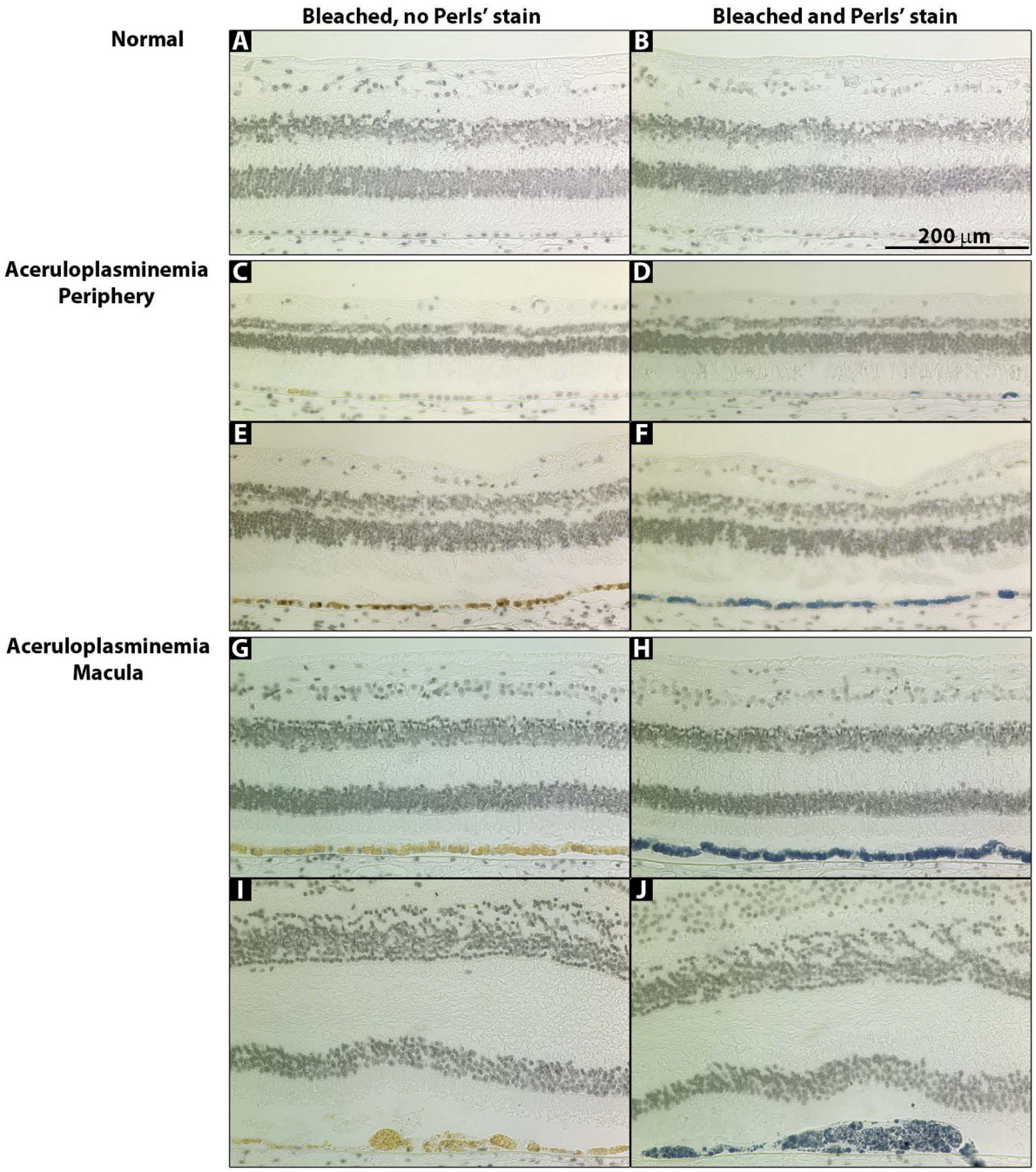

Figure 4. Photomicrographs of macular and peripheral retina sections stained with Perls' Prussian blue stain for iron

(A, C, E, G, I) Bleached sections that were not stained with Perls' stain. (B, D, F, H, J) Bleached sections that were stained with Perls' stain for iron (blue). (A, B) Normal retina. (C–F) aCP peripheral retina. (G–J) aCP macular retina.

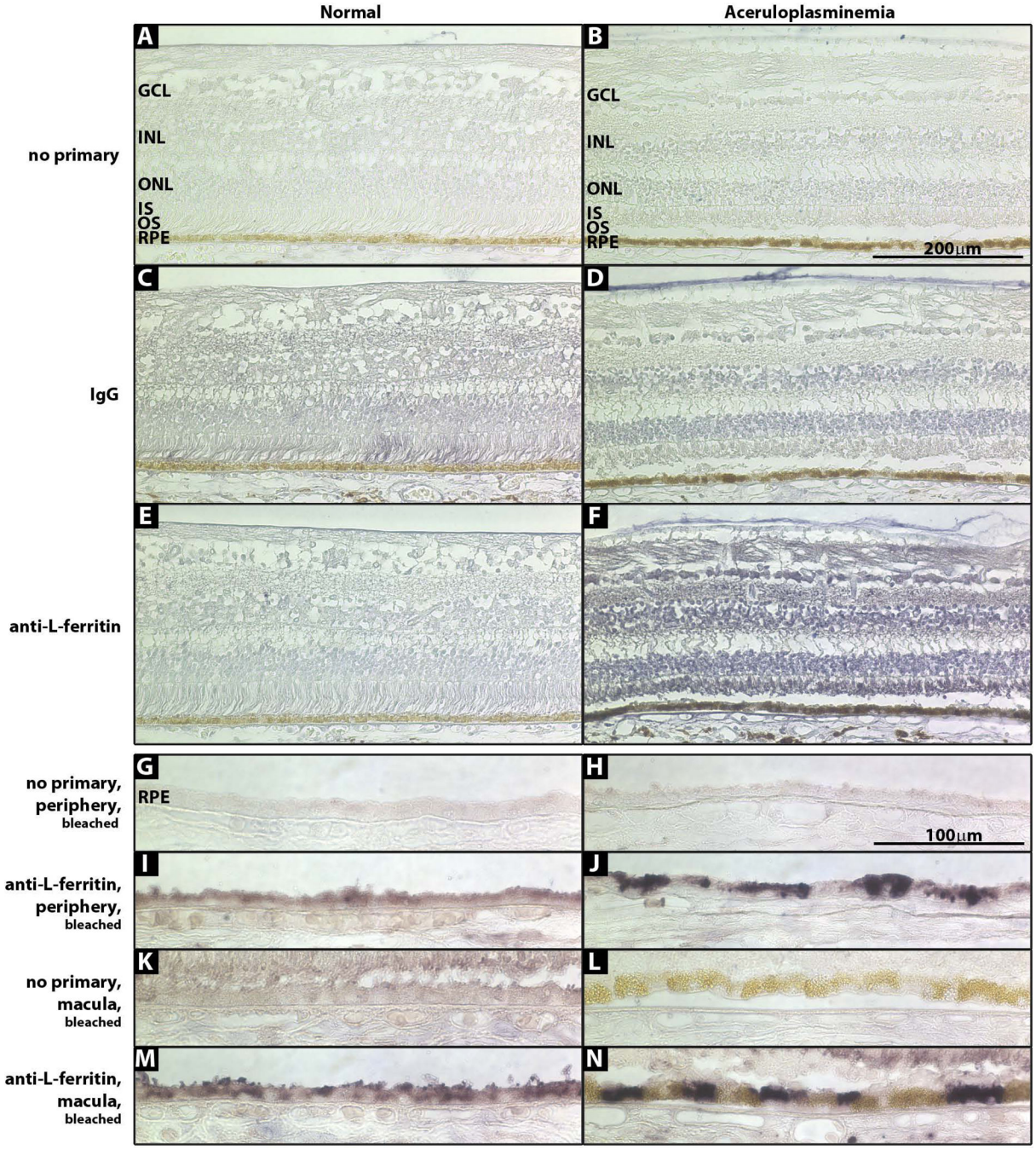

Figure 5. Photomicrographs of normal and aCP retinas immunostained for L-ferritin

(A, B) No primary antibody. (C, D) IgG control. (E, F) L-ferritin. (G–N) sections were bleached prior to L-ferritin stain to remove melanin. (G, H) No primary antibody, peripheral retina. (I, J) L-ferritin, peripheral retina. (K, L) No primary antibody, macula. (M, N) L-ferritin, macula.

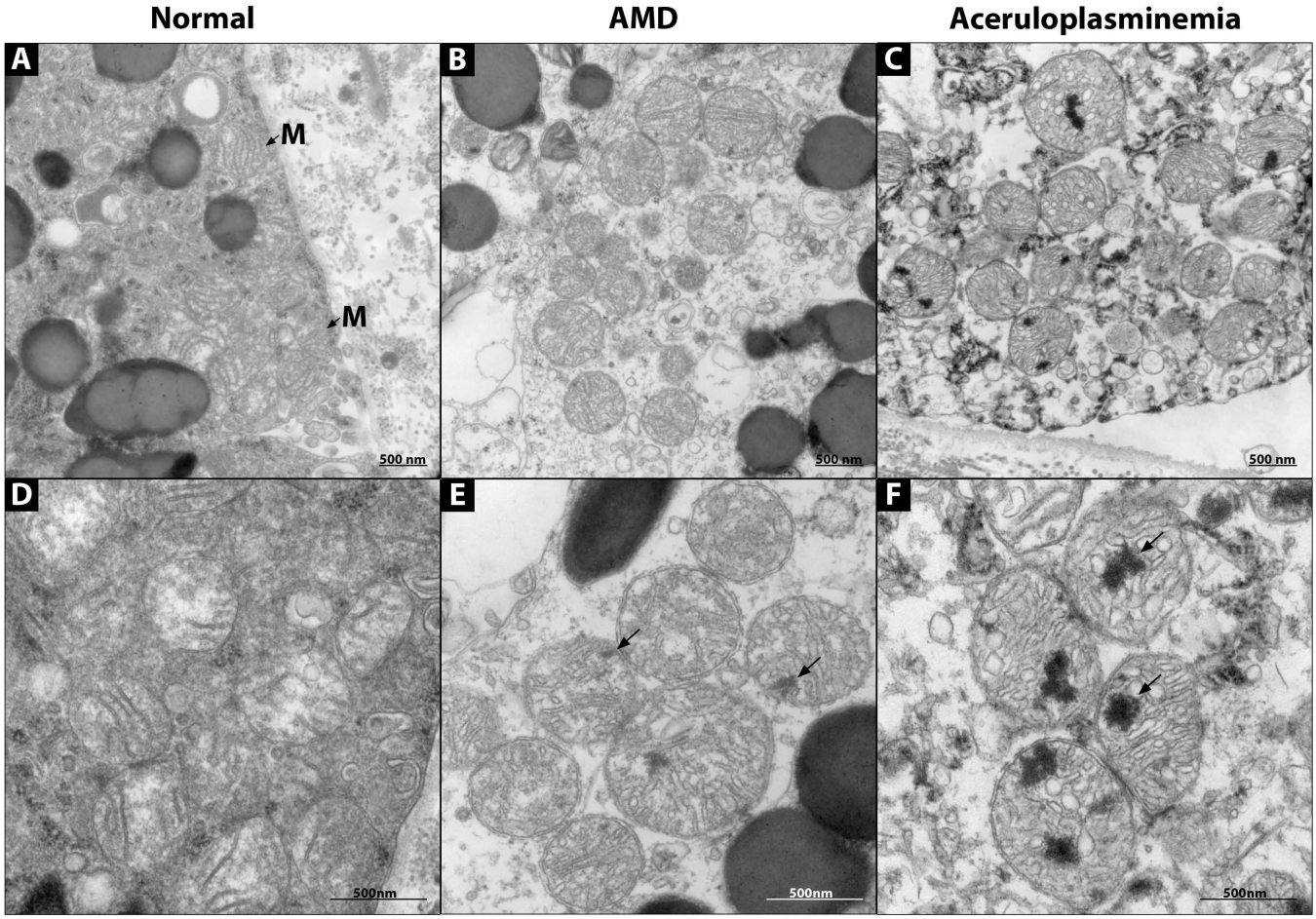

Figure 6. Electron micrographs of RPE mitochondria

(A–C) 30,000× magnification. (D–F) 60,000× magnification. (A, D) Normal RPE. (B, E) AMD RPE. (C, F) aCP RPE. Electron dense inclusions (arrows). Mitochondria (M with arrow).

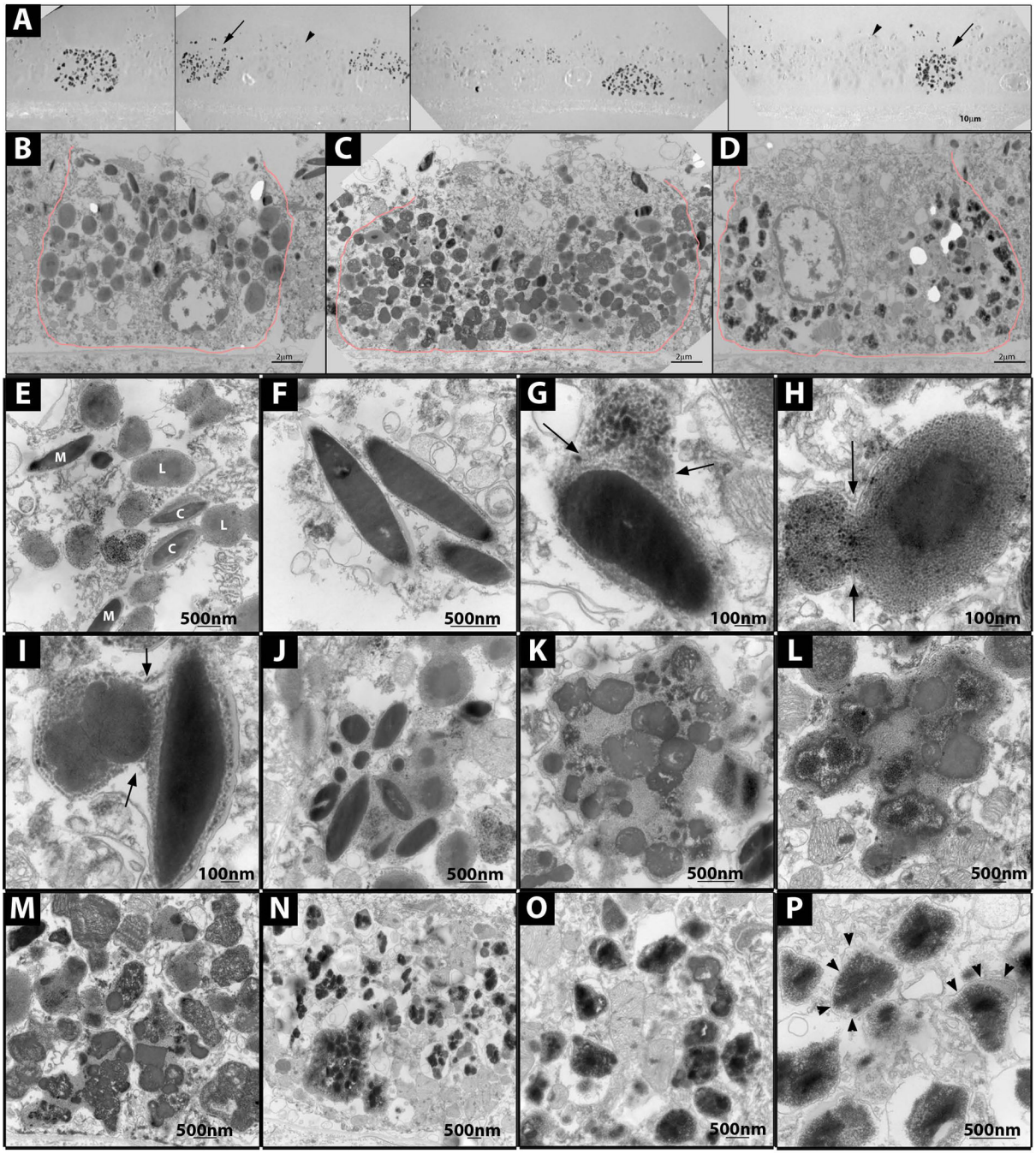

Figure 7. Electron micrographs showing RPE granules and melanosome degradation

(A) Melanosome-rich (arrowhead) and poor (arrow) RPE cells on unstained EM sections. (B) Melanosome-rich cell, stained EM. (C) Intermediated cell, stained EM. (D) Melanosome-poor cell, stained EM. (E) Melanosomes (M), lipofuscin (L) and complex granules (C) in melanosome-rich RPE cell. (F) Normal melanosomes in melanosome-rich RPE cell. (G) Melanosome fusing with lipofuscin or lysosomal granule in melanosome-rich RPE cell. (H) Complex granule fusing with additional lipofuscin granule. (I) Two complex granules fusing in a melanosome-rich cell. (J)Aggregate of melanosomes and lipofuscinoid

material in a melanosome-rich cell. (K,L) Aggregate of melanosomes and lipofuscinoid material, with degrading melanosomes in a melanosome-rich cell. (M)Aggregates of degraded melanosomes and lipofuscinoid material in an intermediate RPE cell. (N) Irregular electron dense granules in a melanosome-poor RPE cell; some granules are aggregated, others are dispersed. (O, P) Irregular electron dense granules in a melanosome-poor RPE cell; limiting membranes (arrowheads).

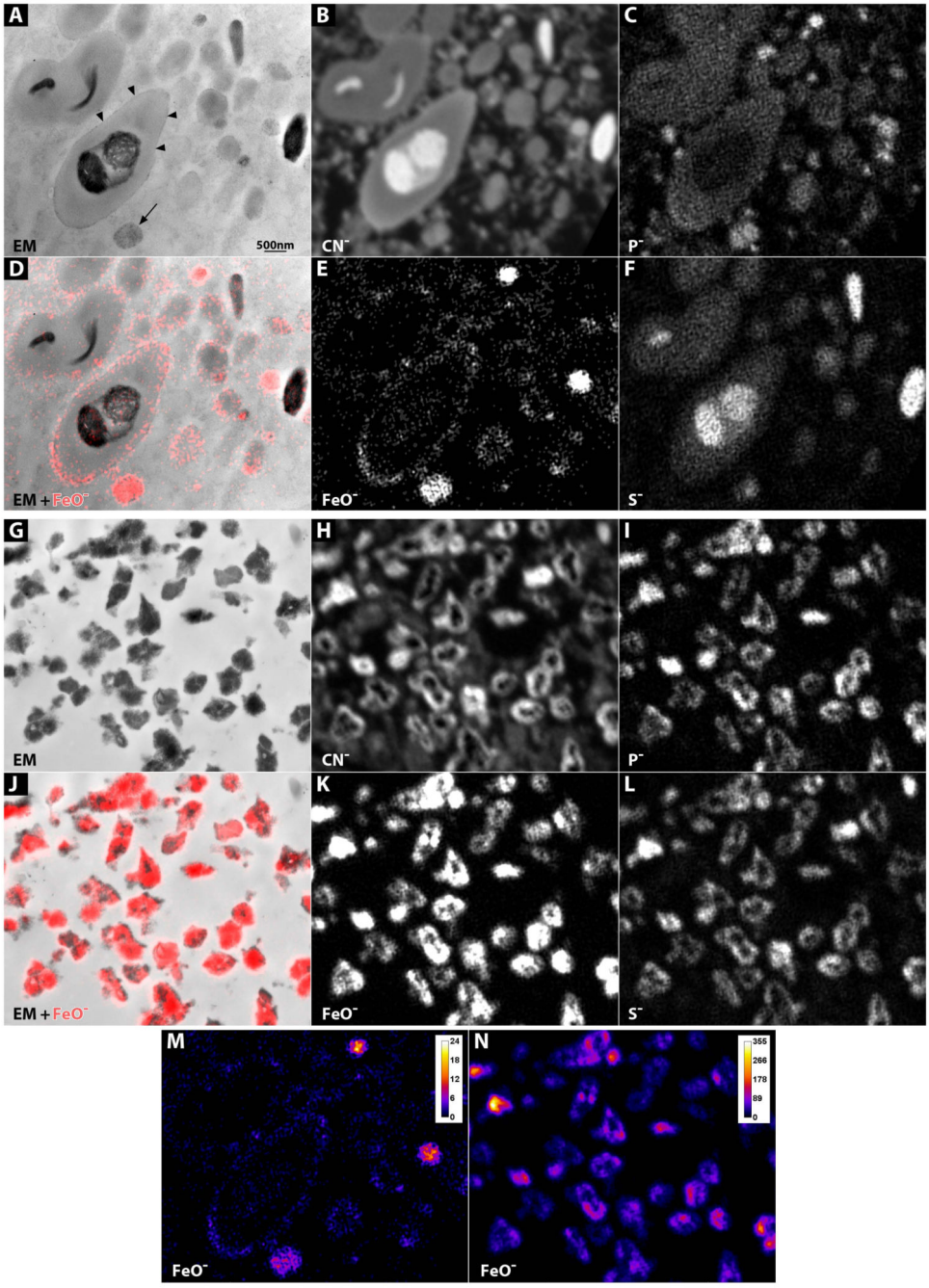

Figure 8. SIMS analysis on melanosome-rich and melanosome-poor RPE cells

(A–F) Melanosome-rich cell. (A)EM of unstained section. Vesicle with electron-dense granular material (arrow). Electron-dense granular rim on a complex granule (arrowheads). (B–F) NanoSIMS analysis of the same section. (B) Carbon-nitrogen. (C) Phosphorus. (D) Iron-oxygen map (red) overlaid onto the EM image. (E) Iron-oxygen. (F) Sulfur. (G–L) Melanosome-poor cell. (G)EM of unstained section. (H–L) NanoSIMS analysis of the same section. (H) Carbon-nitrogen. (I) Phosphorus. (J) Iron-oxygen map (red) overlaid onto the

EM image. (K) Iron-oxygen. (L) Sulfur. (M–N) Iron-oxygen gradient map comparing iron levels in melanosome-rich (M) and melanosome-poor (N) cells.